AFRL-PR-WP-TP-2007-239

STREAMWISE VORTICITY EFFECTS IN A CURVED DIFFUSER WITH SLOT JET FLOW CONTROL (PREPRINT)

S. Todd Bailie and David Car

Fan and Compressor Branch
Turbine Engine Division

JUNE 2006

AIR FORCE RESEARCH LABORATORY
PROPULSION DIRECTORATE
WRIGHT-PATTERSON AIR FORCE BASE, OH 45433-7251
AIR FORCE MATERIEL COMMAND
UNITED STATES AIR FORCE

REPORT DOCUMENTATION PAGE

Form Approved
OMB No. 0704-0188

1. REPORT DATE *(DD-MM-YY)*	2. REPORT TYPE	3. DATES COVERED *(From - To)*
June 2006	Conference Paper Preprint	01 June 2005 – 01 June 2006

4. TITLE AND SUBTITLE
STREAMWISE VORTICITY EFFECTS IN A CURVED DIFFUSER WITH SLOT JET FLOW CONTROL (PREPRINT)

5a. CONTRACT NUMBER
In-house

5b. GRANT NUMBER

5c. PROGRAM ELEMENT NUMBER
N/A

6. AUTHOR(S)
S. Todd Bailie and David Car (AFRL/PRTF)
Jordi Estevadeordal (Innovative Scientific Solutions, Inc.)

5d. PROJECT NUMBER
N/A

5e. TASK NUMBER
N/A

5f. WORK UNIT NUMBER
N/A

7. PERFORMING ORGANIZATION NAME(S) AND ADDRESS(ES)

Fan and Compressor Branch (AFRL/PRTF), Turbine Engine Division
Air Force Research Laboratory, Propulsion Directorate
Wright-Patterson Air Force Base, OH 45433-7251
Air Force Materiel Command
United States Air Force

Innovative Scientific Solutions, Inc.
Dayton, OH 45440

8. PERFORMING ORGANIZATION REPORT NUMBER
AFRL-PR-WP-TP-2007-239

9. SPONSORING/MONITORING AGENCY NAME(S) AND ADDRESS(ES)

Air Force Research Laboratory
Propulsion Directorate
Wright-Patterson Air Force Base, OH 45433-7251
Air Force Materiel Command
United States Air Force

10. SPONSORING/MONITORING AGENCY ACRONYM(S)
AFRL/PRTF

11. SPONSORING/MONITORING AGENCY REPORT NUMBER(S)
AFRL-PR-WP-TP-2007-239

12. DISTRIBUTION/AVAILABILITY STATEMENT
Approved for public release; distribution unlimited.

13. SUPPLEMENTARY NOTES
Conference paper submitted to the 2006 Third AIAA Flow Control Conference. The U.S. Government is joint author of this work and has the right to use, modify, reproduce, release, perform, display, or disclose the work.

PAO Case Number: AFRL/WS 06-1339, 17 May 2006.

14. ABSTRACT
A slot jet is used to increase the diffusion level of a curved, diffusing wind tunnel passage. The passage entrance coincides with the tunnel throat, which has respective Mach and Reynolds numbers of 0.7 and 187000 (based on throat height) and jet Reynolds numbers ranging from 10000 to 22000. Each of four presented configurations uses linear slot jet flow control at the same relative location. Three configurations include co- or counter-rotating vortex generator (VG) fins of varying heights upstream of the slot jet, while the other configuration has no VGs. The configurations are tested for varying flow control input and evaluated primarily on the basis of passage exit total pressure surveys. At baseline conditions (minimum slot jet flow), the shorter VG designs were found to provide some diffusion enhancement and loss reduction compared to the non-VG configuration, whereas the tall counter-rotating VGs exhibit an increase in loss. With the addition of slot jet flow, all configurations showed an initial decline followed by a net increase in performance of similar magnitude, with choked slot jet flows tending to lead to flow instabilities. Upon further increases in slot jet flow, all configurations eventually achieved a stable flow pattern. A noteworthy change in the flow pattern, with substantially improved uniformity, is documented near 6% flow control input and will be the subject of more detailed investigation.

15. SUBJECT TERMS
flow control, axial compressor, stator, vortex generator, slot jet

16. SECURITY CLASSIFICATION OF:			17. LIMITATION OF ABSTRACT:	18. NUMBER OF PAGES	19a. NAME OF RESPONSIBLE PERSON (Monitor)
a. REPORT	b. ABSTRACT	c. THIS PAGE			Steven L. Puterbaugh
Unclassified	Unclassified	Unclassified	SAR	24	19b. TELEPHONE NUMBER *(Include Area Code)* N/A

Standard Form 298 (Rev. 8-98)
Prescribed by ANSI Std. Z39-18

Streamwise Vorticity Effects in a Curved Diffuser with Slot Jet Flow Control

S. Todd Bailie* and David Car*

Air Force Research Laboratory, WPAFB, OH, 45433, USA

Jordi Estevadeordal†

Innovative Scientific Solutions, Inc., Beavercreek, OH, 45440, USA

A slot jet is used to increase the diffusion level of a curved, diffusing wind tunnel passage. The passage entrance coincides with the tunnel throat, which has respective Mach and Reynolds numbers of 0.7 and 187000 (based on throat height) and jet Reynolds numbers ranging from 10000 to 22000. The throat aspect ratio (height-to-span) is approximately 7:1 and the diffusing section of the passage has an approximate radius of curvature of 5.08 cm for the convex surface. Each of four presented configurations uses linear slot jet flow control at the same relative location. Three configurations include co- or counter-rotating vortex generator (VG) fins of varying heights upstream of the slot jet, while the other configuration has no VGs. The configurations are tested for varying flow control input and evaluated primarily on the basis of passage exit total pressure surveys. At baseline conditions (minimum slot jet flow), the shorter VG designs were found to provide some diffusion enhancement and loss reduction compared to the non-VG configuration, whereas the tall counter-rotating VGs exhibit an increase in loss. With the addition of slot jet flow, all configurations showed an initial decline followed by a net increase in performance of similar magnitude, with choked slot jet flows tending to lead to flow instabilities. Upon further increases in slot jet flow, all configurations eventually achieved a stable flow pattern, though three configurations produced highly asymmetric exit flow distributions. Only the tall counter-rotating VG configuration produced a symmetric exit flow at high flow control inputs. A noteworthy change in the flow pattern, with substantially improved uniformity, is documented near 6% flow control input and will be the subject of more detailed investigation.

I. Introduction

Flow control for application in axial compression systems has become a very active research topic for the last few decades.[1–6] It has the potential to open the design envelope for axial compressors to higher loading levels for a given compressor stage, translating into higher overall pressure ratios for improved thrust specific fuel consumption (TSFC). Increased loading levels may also yield higher thrust-to-weight (T/W) ratios by reducing turbine engine axial length for a given pressure ratio. This is of particular interest since, as shown in Reference 7, engine thrust-to-weight ratios have practically leveled off since the 1970s.

The Compressor Aero Research Lab (CARL) at the Air Force Research Laboratory (AFRL) has designed and built a small scale wind tunnel facility to test candidate flow control concepts for use in axial compression systems.[8] The facility is capable of Mach 0.7 continuous flow and is modular in design, with generous optical access for acquiring both Digital Particle Image Velocimetry (DPIV) and Pressure-Sensitive Paint (PSP) data. It was designed to quickly vet candidate concepts at a low cost prior to larger scale implementation. A key goal at CARL is to increase the diffusion capability of compressor stator passages to allow increased compressor rotor loading levels. Currently, concepts that are being evaluated are variations on a slot jet configuration.

*Aerospace Engineer, AFRL/PRTF, 1950 Fifth Street Bldg 18, WPAFB, OH 45433, AIAA Member.

†Mechanical Engineer, ISSI, Beavercreek, OH 45440, AIAA Member.

Slot jets for flow control have been considered by researchers for over 50 years.[9] This configuration can be found in Coanda-type applications[10] as well as diffusing passages to control separation.[3,9,11–13] The slot jet strategy does not appear to be popular as a method for accomplishing this task since it suffers from instabilities and implementation difficulties over skewed, discrete jet blowing and passive techniques (such as vortex generators) which capitalize on streamwise vorticity production.[14–17] But some of these difficulties are being addressed as recent research has shown that unsteady forcing of turbulent, planar, shear flows increases the turbulent dissipation in the shear layer and may result in a more efficient mixing process.[18]

This paper provides an initial experimental comparison of steady, linear slot jet flow control effectiveness in a curved diffusing passage with and without streamwise vorticity augmentation. Diffuser exit total pressure surveys are used to evaluate a baseline slot jet and three vortex generator configurations in terms of flow patterns, overall losses, and flowfield uniformity.

II. Experimental Setup

A. Facility

The Flow Control Augmented Diffusion (FCAD) wind tunnel facility is comprised of three major elements: the wind tunnel itself, the primary flow source and a secondary flow source used for flow control implementation.

1. FCAD Tunnel

The FCAD wind tunnel is an atmospheric in-draft design. After passing through a bellmouth and flow straightener, the airflow accelerates through a converging inlet of roughly 12:1 area contraction to a rectangular throat, 1.5 x 10.2 cm (0.6 x 4.0 in). The throat, typically operated at Mach 0.7, is the beginning of the curved diffuser test section. The diffuser geometry is based on aggressive goals for an axial compression system. The diffuser passage has an exit-to-throat area ratio of 2.92, a flow turning angle of 70 degrees, with suction (convex) side radius of curvature nearly constant at 50.8 mm (2.0 in).

Following the diffuser is a sudden expansion into a rectangular settling chamber. An adaptor piece guides the flow from the settling chamber into a flexible 7.6 cm (3 in) diameter duct connected to the primary flow source. Figure 1 illustrates the basic flowpath from the inlet (at right) to the settling chamber (left). The area ratio distribution in the diffusing section, determined by projecting the normals of the convex surface to the concave surface and dividing by the throat area, is shown in Figure 2 as a function of the percentage of convex surface coordinate from the throat to exit. The static-to-total pressure ratio, shown in Figure 2, is calculated using this area distribution and one-dimensional, ideal gas dynamics. This area distribution results in a fairly linear and aggressive pressure gradient from approximately 10-50% of the surface coordinate and then gradually reduces toward the exit. The application of the more severe gradient early in the diffusion process is a more effective strategy since the boundary layer health is general better and able to negotiate a more severe pressure gradient.[19]

Because present research goals include identification of key physical mechanisms relating diffusion and flow control, emphasis has been placed on measurement techniques that can resolve details of the overall flowfield. Optical techniques, especially Digital Particle Image Velocimetry (DPIV), were chosen to fill this need. The tunnel was accordingly designed with optical access as a priority. The top and bottom walls are transparent acrylic sheets, and sandwiched in between are wall segments with height of 10.2 cm (4 in). Defining the convex (suction) side of the curved diffuser test section is a readily replaceable aluminum module for testing various flow control concepts. The inlet contraction and pressure (or concave) side of the diffuser passage are machined from a single block of acrylic to maintain a smooth and dimensionally accurate profile, with all surfaces polished to restore high clarity for optically-based measurements.

2. Primary Flow System

To permit an atmospheric inlet, the FCAD wind tunnel is run in a suction configuration. An automative centrifugal supercharger, with self-contained speed-increasing gearbox, provides the suction source. A 37 kW (50 hp) 3-phase AC induction motor drives the supercharger through a cogged belt system. A variable frequency drive (VFD) unit is used to precisely control the motor and match the desired tunnel flow conditions. Unlike typical cascade wind tunnels, the target Mach number can typically be maintained indefinitely

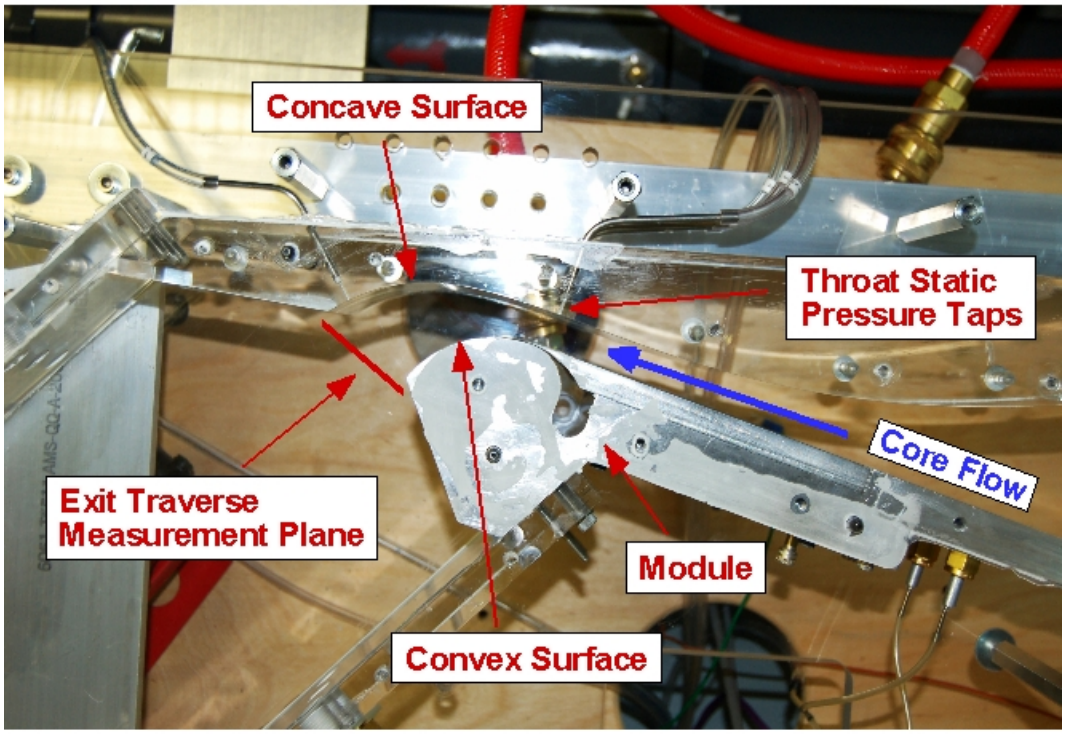

Figure 1. Top view of the FCAD wind tunnel test section

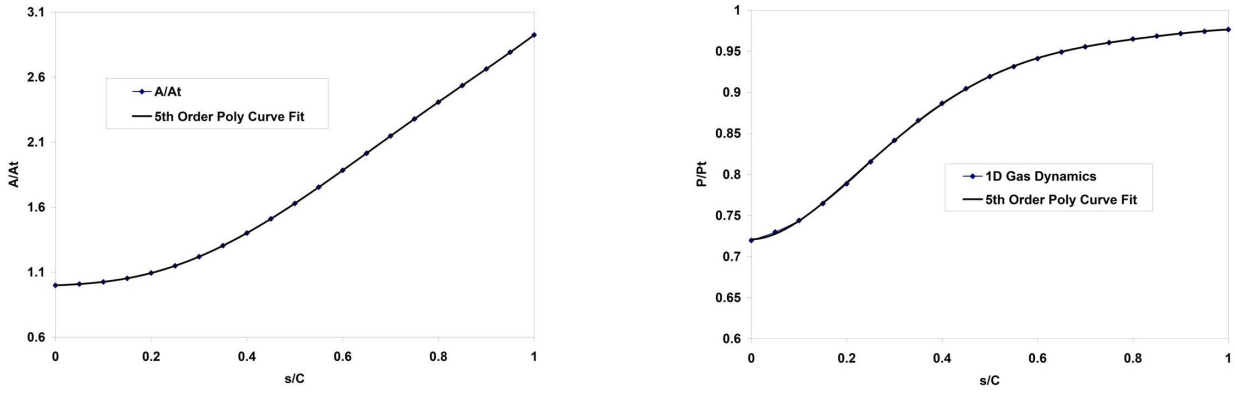

(a) Area Distribution

(b) Static-to-Total Pressure Ratio Distribution

Figure 2. Characteristics of the FCAD tunnel Diffusing Test Section

and repeated within 0.3% of the intended value. Flow is exhausted from the supercharger through a metal duct to the exterior of the building.

3. Flow Control System

Flow control supply air is available in the form of suction, blowing, or both. A 7.5 kW (10 hp) oil-less vane compressor is used to provide flow control air up to 6% of the primary stream massflow at the normal 0.7 Mach throat condition. A settling chamber is used to reduce discharge pressure oscillations. After metering, the flow is routed to an internal plenum in the flow control module. In testing to date, only blowing has been used for active flow control. However, the compressor can be readily plumbed for suction or a combination of both. As with the primary flow system, the vane compressor is precisely controlled by a VFD unit.

B. Measurements

The facility has been designed for a variety of measurement techniques. In addition to numerous steady pressure and temperature measurements, optical techniques can be used to non-intrusively document the flow behavior. Digital Particle Image Velocimetry (DPIV) is used to obtain instantaneous flow visualization and vector fields, as well as the average flowfield. Pressure Sensitive Paint (PSP) and rake probe traverses are used to map suction surface static and diffuser exit total pressures, respectively. Primary stream massflow rates are determined with a Venturi flow meter, and an orifice meter is used to quantify any flow control massflow added or removed from the primary stream.

The exit traverse was described in Ref. 8, but is restated here for completeness. Total pressure measurements were taken at the exit of the passage using a 5 probe rake oriented pitchwise (convex to concave surfaces) and traversed spanwise. The rake is typically indexed in 5% pitch increments to obtain 20 interlaced positions from 0% to 95% pitch and traversed through spanwise increments of 3.125% for a total of 580 measurement locations. One data point consists of an average of 100 samples taken at 800 Hz. A total of 10-20 such data points were taken at each location and used for statistical calculations. Effectively, this eliminated any high frequency unsteadiness and signal noise in the measurements, but still allowed low frequency fluctuations to be captured.

III. Definitions and Approximations

A brief overview of some of the parameters used later in this paper will be outlined here. The loss parameter, ζ_{Pt}, is defined as the area-averaged total pressure deficit as a fraction of inlet total pressure as follows:

$$\zeta_{Pt} = \frac{1}{A}\int_0^A \frac{P_G}{P_0} dA \tag{1}$$

where P_G is the measured gage pressure referenced to the facility inlet total pressure, P_0. The area of integration, A, is the actual flow area mapped during each exit survey. This loss parameter will be used as a measure of global loss throughout the paper and as a measure of effectiveness of the flow control technique.

The standard deviation for the exit traverse measurements presented later is defined as:

$$\sigma_x = \sqrt{\frac{\sum (x-\bar{x})^2}{n-1}} \tag{2}$$

where n is the number of samples taken. This standard deviation will be used as a general indication of the level of low frequency unsteadiness in the exit total pressure measurements as observed during the experiment. Data points are obtained about once every second, with each point being an average of 100 samples taken at 1 kilohertz.

The flow fraction is defined simply as the ratio of secondary (i.e. flow control) mass flow to primary (i.e. core) mass flow. This is determined from direct measurements in the experiment. For some comparisons, it is desirable to use the momentum flux ratio, which is the ratio of secondary flow momentum to core flow

momentum. It is approximated from static and total pressure measurements obtained in the experiment as follows:

$$\begin{aligned} c_\mu &= \frac{\rho_j V_j^2}{\rho_c V_c^2} \\ &= \left(\frac{P_{t_j}}{P_{t_c}}\right)\left(\frac{M_j}{M_c}\right)^2 \left(\frac{1+\frac{\gamma-1}{2}M_c^2}{1+\frac{\gamma-1}{2}M_j^2}\right)^{\frac{\gamma}{\gamma-1}} \end{aligned} \tag{3}$$

where P_t is total pressure and M is the Mach number. The subscripts c and j refer to the core and slot jet flow conditions, respectively. The Mach number is determined using the isentropic total-to-static pressure ratio, with static measurements taken at the nearest relevant tap location.

The jet and tunnel Reynolds numbers are approximated in similar fashion to c_μ as follows:

$$\begin{aligned} Re &= \frac{\rho V L}{\mu} \\ &= \frac{\gamma P_t}{\sqrt{\gamma R T_t}} \frac{L}{\mu} \frac{M}{\left(1+\frac{\gamma-1}{2}M^2\right)^3} \end{aligned} \tag{4}$$

where μ is the viscosity and L is the length scale for the tunnel or slot jet. The total pressure used for the slot jet Reynolds number calculation was the measured plenum supply pressure of the slot jet. The core flow total pressure was approximated as the measured atmospheric pressure. The length scale for the tunnel and slot jet is the tunnel throat height (15.24 mm) and jet height (typically 0.51 mm), respectively. With the tunnel running at design conditions and using standard day conditions, the Reynolds number is approximately 188000. The slot jet Reynolds number for the tested configurations ranged from 10000 to 22000.

IV. Test Configurations

Four different configurations are evaluated in the present work. The flow control module of the FCAD tunnel uses a common base block, as shown in Figure 3, and is reconfigured by replacing the upper plate with different designs. Each of the present configurations uses linear slot jet flow control at the same relative location, issuing from between the upper plate and base block. Shim washers were used as needed for each case at varying locations during module assembly to maintain a spanwise-uniform slot jet height, as close as feasible to the intended height of 0.508 mm (0.020 in). Actual slot heights were measured by feeler gages, with uncertainty estimated to be ±0.013 mm (0.0005 in).

Two configurations include counter-rotating vortex generator (VG) fins of varying heights just upstream of the slot jet, while one configuration makes use of co-rotating VGs. The fourth version has no VGs and serves as the baseline configuration. The configurations are tested for varying flow control input and evaluated primarily on the basis of passage exit total pressure surveys.

A. Linear Slot Jet

The spanwise linear slot jet (LSJ) module is shown in Figure 3. A 5 degree chamfer exists on the end of the removable upper plate, reducing the lip thickness at the slot jet to 0.127 mm (0.005 in). This metal thickness is 25% of the jet height and was found to be reasonable, resulting in an effective interaction between the slot jet and the core stream as outlined in Ref. 8. This metal thickness to jet height ratio is maintained as close as possible for all the modules outlined in this paper. As assembled for testing, the slot height of the LSJ-only configuration was measured as 0.508 mm (0.020 in) across the span.

B. With Counter-Rotating VGs

An spanwise arrangement of flat-plate vortex generator fins was developed such that repeating pairs of counter-rotating streamwise vortices would be generated above the core flow surface of the flow control

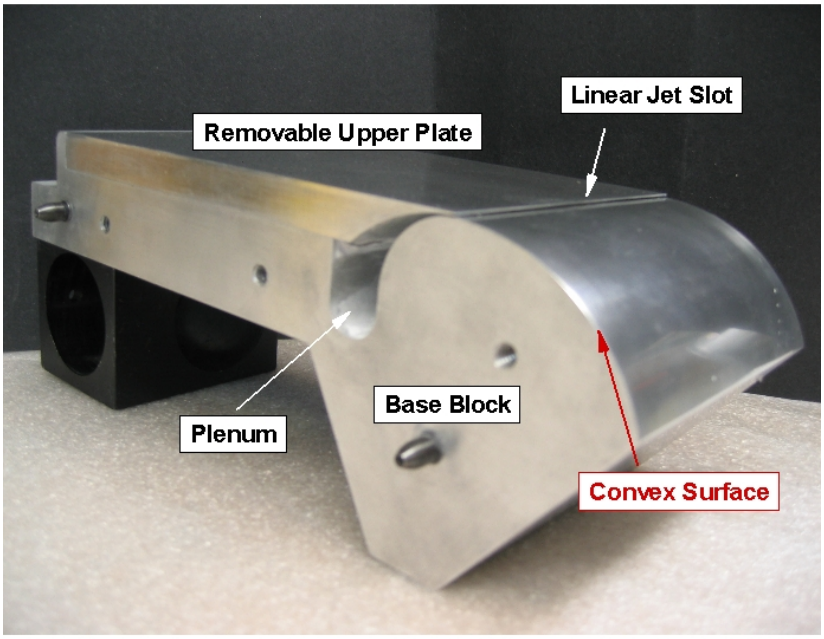

Figure 3. Linear Slot Jet Module

module, just upstream of the linear slot jet and its lead-in chamfer. Care must be taken when using counter-rotating vortices due to the induced motion of the vortices on one another, and good references on this subject are given by Pearcey[9] and Kuethe and Chow.[20] The counter-rotating VG arrangement was designed, based on the detailed methodology described in Ref. 8, with the intent that the induced motion of the vortices would be toward the slot jet and the convex surface. The selected design utilizes rectangular fins normal to the surface and inclined at 25° to the flow direction, with chord of 3.96 mm (0.156 in). The distance between trailing edges of paired fins, d, is 3.77 mm (0.148 in) while the a spacing of $4.5d$ between neighboring pairs is used.

Two configurations of counter-rotating VGs, differing only in height, were used in the present work. The VG heights are specified as a percentage of the local boundary layer (BL) thickness, which was estimated to be 2.54 mm (0.100 in) with no VGs by two-dimensional CFD analysis. An initial VG height of 3.81 mm (0.150 in), or 150% of the BL thickness, was fabricated. Subsequently a new configuration was intended to have VGs of half-height, but a drafting error led to a quarter-height of 0.965 mm (0.038 in), or 38% of the BL height. These respective configurations are subsequently referred to as "Counter-VG-150" and "Counter-VG-38" and are shown in Figure 4.

The measured slot height for the Counter-VG-150 module was 0.508 mm (0.020 in) across the span, whereas, owing to manufacturing variations, the Counter-VG-38 module measured 0.610 mm (0.024 in) at the slot midspan and 0.584 mm (0.023 in) at the slot ends. It was anticipated that the Counter-VG-38 configuration, with its larger, non-uniform slot height and short VG height, would likely show reduced flow control effectiveness.

C. With Co-Rotating VGs

A co-rotating VG configuration was also developed by selectively removing individual VG fins from the counter-rotating configuration. The central "V-shaped" VG pair was maintained at midspan, but the inboard fin of all other pairs was removed as visible in Figure 4. Thus a single counter-rotating vortex pair is produced at midspan, but on either side of midspan a row of co-rotating vortices is produced. Co-rotating vortices do not induce motion on each other, but if they are in close proximity to a solid boundary they will migrate along the surface. The present VG arrangement was such that any vortex migration would be outward, that

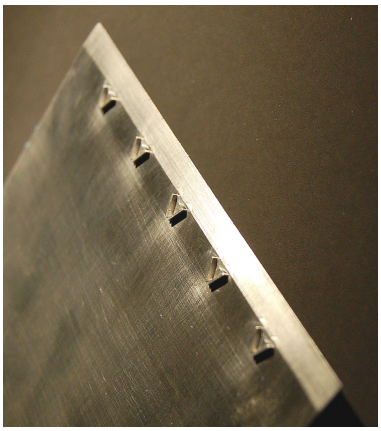

(a) Counter-Rotating VGs, 38% BL height

(b) Counter-Rotating VGs, 150% BL height, with Base Block

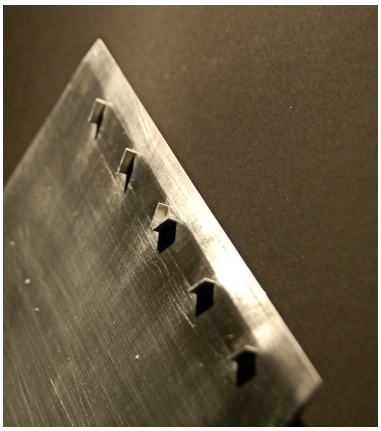

(c) Co-Rotating VGs, 75% BL height

Figure 4. Vortex Generator test configurations, oriented for relative core flow from lower-left to upper-right of the images.

is from the midspan towards the endwalls of the diffuser passage. The underlying assumption was that this arrangement might improve endwall flow behavior, which had been previously observed[8] to be problematic.

The height of the co-rotating VGs was chosen as 1.91 mm (0.075 in), or 75% of the BL thickness, and this configuration is referred to as "CoRot-VG-75". The measured slot height for the CoRot-VG-75 module was 0.533 mm (0.021 in) across the span.

V. Results and Discussion

This section is divided into two parts, with the first being devoted to observations and limited physical interpretation of the flow behavior noted during testing of the various configurations. This portion primarily focuses on the total pressure distributions measured at the exit of the diffusing passage. In the second part, the different configurations are directly compared based on overall performance metrics, including loss integrations of the pressure distributions.

A. Flow Behavior

The morphology of the diffuser exit total pressure patterns under varying slot jet flow control input is depicted for the four test configurations in Figures 5, 6, 7 and 8, which require some explanation. The lower contour plot in each subfigure is the locally-averaged exit gage total pressure measurement divided by the inlet total pressure. The area-averaged value over the measurement region is shown as ζ_{Pt} below the contour bar and defined in Equation (1). The grey box surrounding the lower plot signifies the actual flow domain, so the reader can see clearly where the measurements were taken in relation to the boundaries of the diffuser exit.

The three dimensional surface projected above this plane is colored according to the same measurement as the bottom plot, but with a topographical view of the standard deviation for all the data points taken at each location. Thus the vertical scale is the standard deviation of the normalized gage total pressure measurements. This calculation again uses the inlet total pressure (atmospheric) for normalization and is defined in Equation (2). The convex and concave surfaces are labeled to orient the viewer and the maximum non-dimensional standard deviation in the figure is given below the contour bar as σ_{max}. The solid black line in the lower figure marks the midspan location of the passage. Each subfigure is labeled with a caption showing the flow control fraction, f, which is the ratio of the secondary (i.e. slot jet) massflow to the primary (i.e. tunnel inlet) massflow. The same scales are used throughout these figures for direct comparison.

1. *Linear Slot Jet*

Figure 5 shows the exit total pressure traverse data for the LSJ configuration with 0.4, 2.0, 3.0, 4.0, 4.5 and 5.0% flow control fractions. The reader should note that data was not collected at 0% as the desired baseline condition. When no flow was allowed to issue from the flow control slot, a strong acoustic tone was generated, presumably due to a slot cavity resonance. This tone was sufficiently loud to cause concerns of structural fatigue failure for the thin-lipped aluminum extension of the module upper plate.

This condition was thus avoided, and a 0.4% minimum amount of flow was allowed to bleed through the slot in order to quell the resonance. Since the tunnel is operated in a vacuum configuration, no additional power input was required to generate this small flow. It is important to note that because of losses associated with constricting this secondary flow, the corresponding slot jet flow had a much lower total pressure than that of the core stream. In fact, all of the present configurations required a slot jet flow fraction of 2.6% or greater to match the secondary stream total pressure to that of the incoming primary stream.

At 0.4% flow fraction, the exit total pressure distribution is seen to be very two-dimensional (i.e. effectively uniform in the spanwise direction). As the slot jet flow fraction is increased, the exit total pressure traverse shows the loss reduction in the midspan region, but still a significant amount of total pressure loss at the endwalls. Above 2.0% flow fraction the pressure distribution becomes increasingly three-dimensional, as the high total pressure fluid (colored red) is drawn towards the convex side. There is also a growing degree of asymmetry and eventually, around the 5.0% case, the high total pressure core shifts dramatically to one side of the passage. This change in the flowfield affected the bulk flow enough that substantial distortion was seen across the tunnel static pressure taps.

It should also be noted that the 5.0% data was taken with half the spatial resolution of the other conditions, which is evident from the coarser nature of the unstructured grid. As the flow fraction was increased to 5.0%, the overall flowfield became bi-stable, switching between two distinct modes. Since this produced a more unsteady flowfield, additional data points were taken at each location. Subfigure [f] of Figure 5 shows only what is referred to as "Mode 2", which was the dominant mode during testing (i.e. the vast majority of data points matched this pattern). This data was filtered on the throat Mach number, since it became extremely assymetric during the occurrence of this mode. Insufficient data was available to clearly characterize the initial mode, but it is assumed to be equivalent to the pattern of the 4.5% case.

As shown, this mode results in the flowfield favoring one side of the tunnel, generally taken to be an undesireable condition. Though no LSJ exit surveys were conducted above 5%, the throat taps indicated a stabilization into the skewed flow pattern for increasing flow fraction. The reason for this shift in the pattern is not yet clear, and future DPIV tests may be used to determine the details of this skewed flowfield.

2. *With Co-Rotating VGs, 75% BL height*

Figure 6 provides the exit total pressure traverse data for the CoRot-VG-75 configuration at 0.0, 2.0, 2.6, 3.0, 3.5 and 4.0% flow control fractions. At 0.0% flow control, the flowfield has a more three-dimensional shape than is evident at 2.0%, as well as regions of substantially higher unsteadiness (indicated by the local standard deviation values) than the nonzero flow fractions. Three-dimensionality then increases above 2.0%, with asymmetry and small-scale irregularities becoming apparent.

At 4.0% and above, a strongly asymmetric skewing of the flowfield is seen. This appears to be similar in character to the LSJ at 5.0% and above, but the low loss region is skewed to the opposite side. The reason for this skewing is again left for future interpretation.

3. *With Counter-Rotating VGs, 38% BL height*

The exit surveys for the Counter-VG-38 configuration are provided in Figure 7 for 0.0, 2.0, 3.0, 4.0, 4.9 and 6.1% flow control fractions. The general trends of the flow pattern morphology appear to be very similar to those of the LSJ in Figure 5, again eventually leading to a skewing of the flow to one side. In contrast, the baseline and 2.0% exit distributions are more three-dimensional than their LSJ-only counterparts. Some other slight differences are apparent, but it seems that the 38% BL height VGs may be too short to substantially alter the flow behavior.

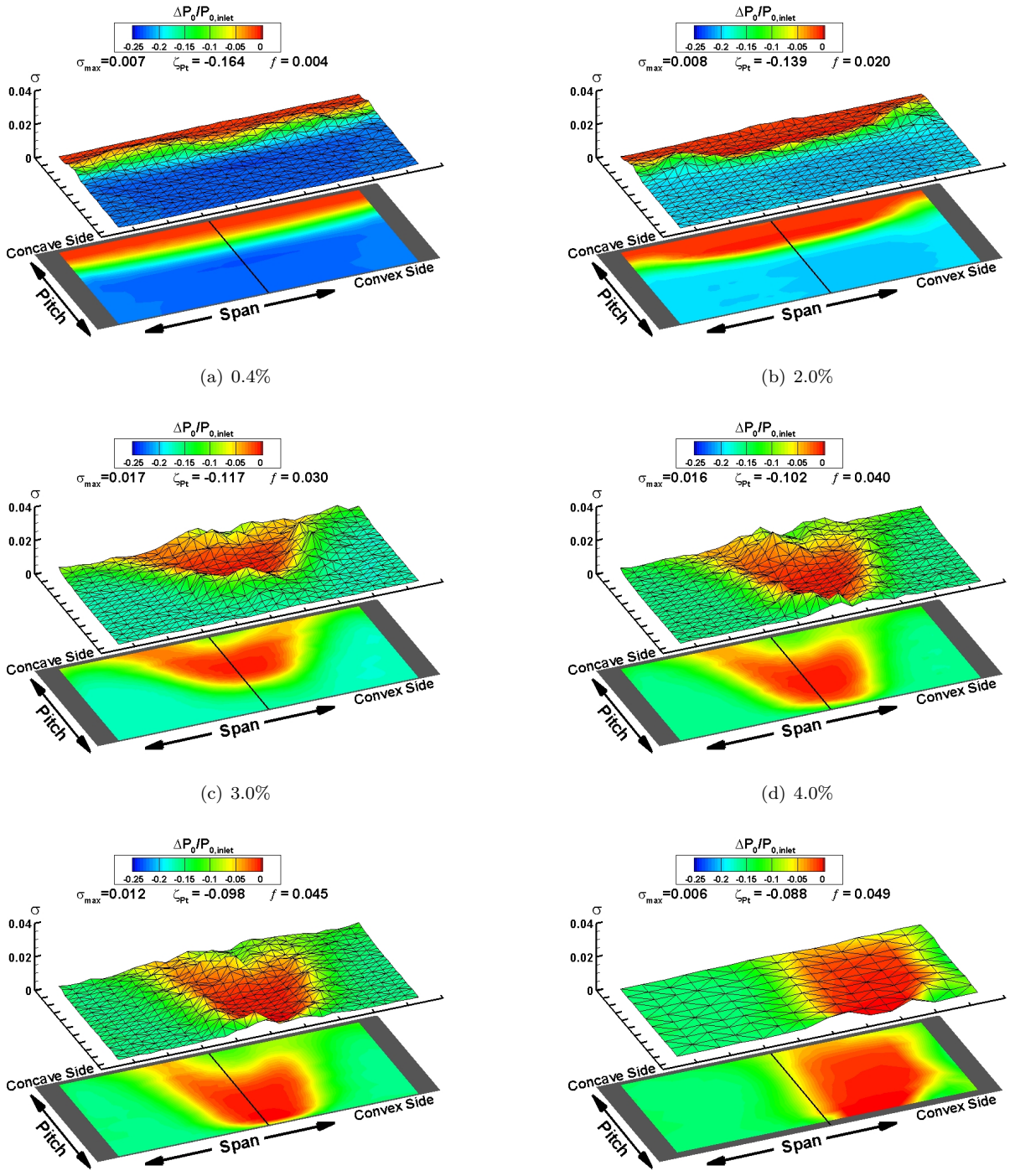

(a) 0.4%

(b) 2.0%

(c) 3.0%

(d) 4.0%

(e) 4.5%

(f) 5.0% Mode 2

Figure 5. Contours of Exit Gage Total Pressure Ratio for varying Linear Slot Jet Flow Control.

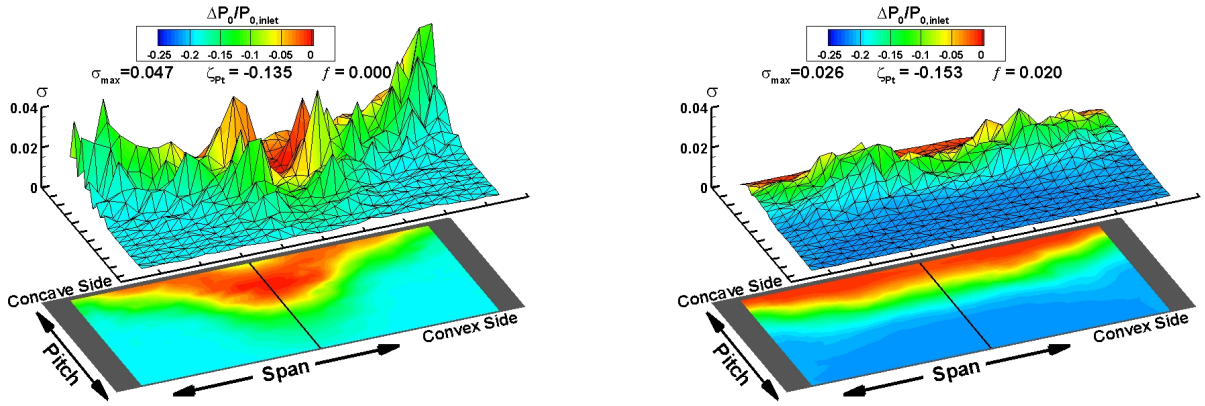

(a) 0.0%

(b) 2.0%

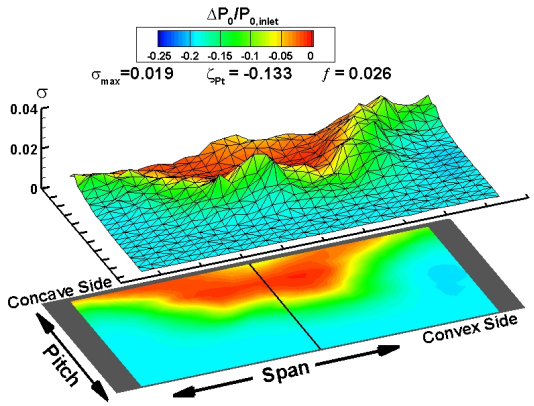

(c) 2.6%

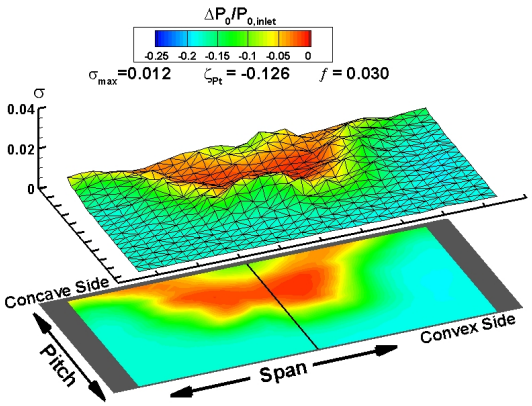

(d) 3.0%

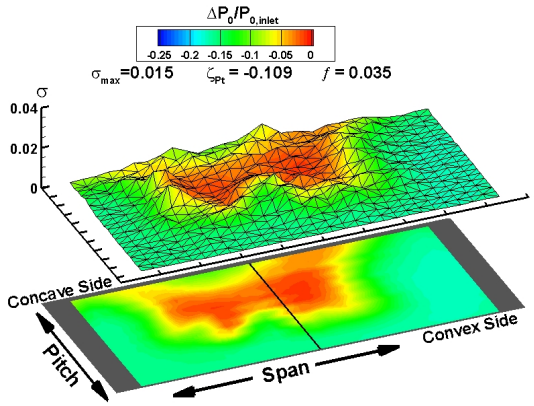

(e) 3.5%

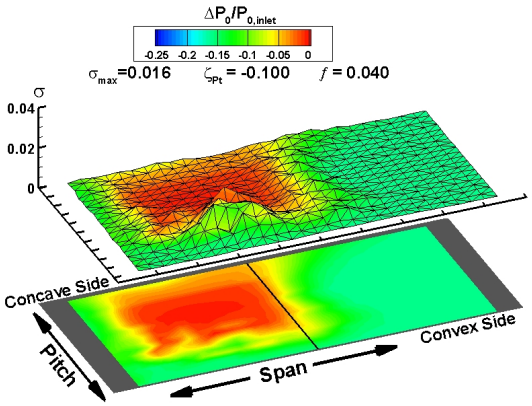

(f) 4.0%

Figure 6. Contours of Exit Gage Total Pressure Ratio for varying Flow Control with Co-Rotating VGs (75% BL height).

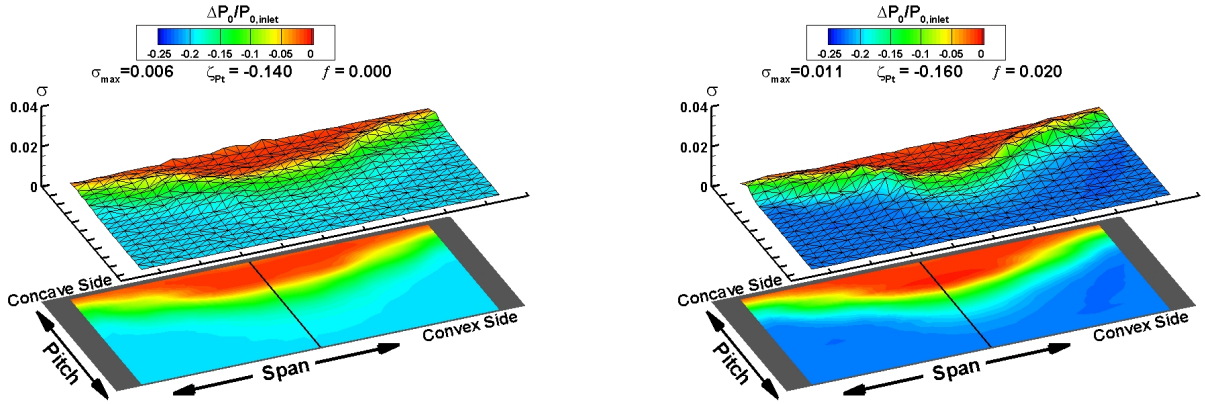

(a) 0.0% (b) 2.0%

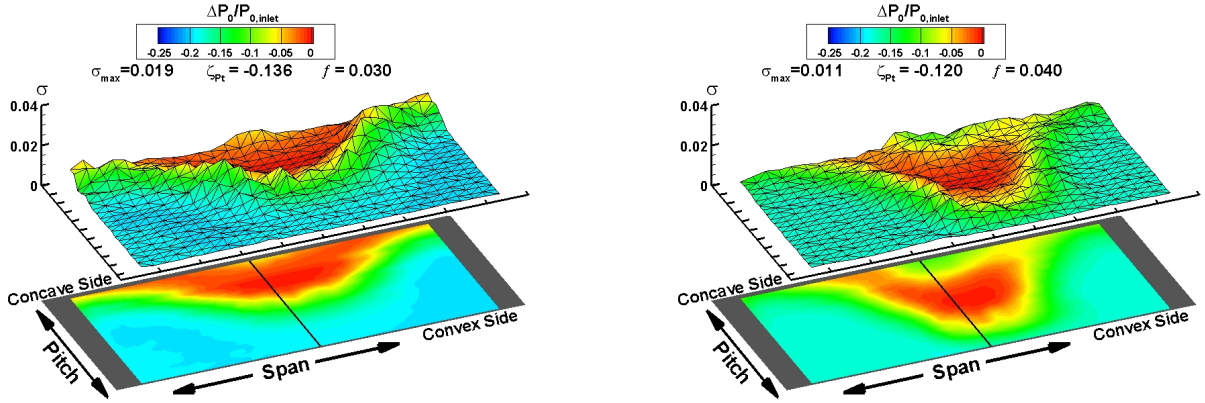

(c) 3.0% (d) 4.0%

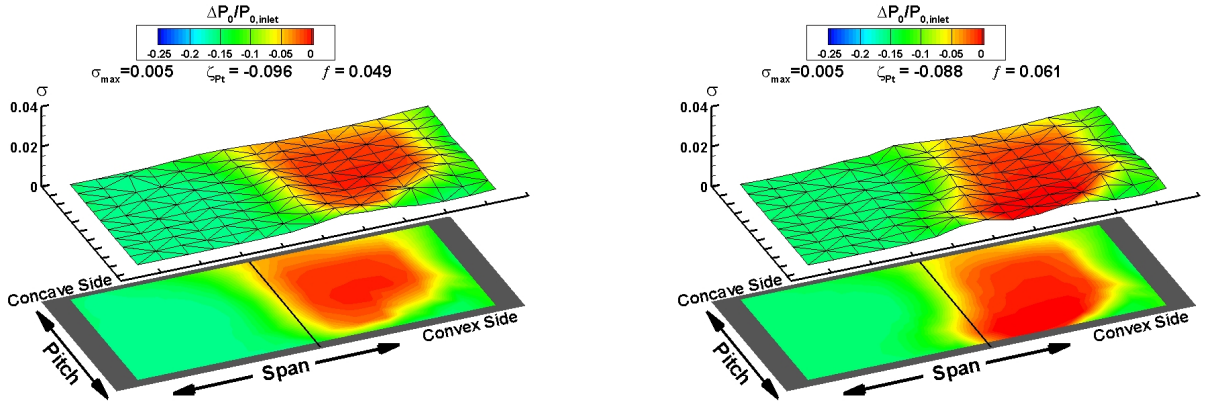

(e) 4.9% (f) 6.1%

Figure 7. Contours of Exit Gage Total Pressure Ratio for varying Flow Control with Counter-Rotating VGs (38% BL height).

4. With Counter-Rotating VGs, 150% BL height

Figure 8 provides the exit surveys for the Counter-VG-150 configuration, operated at flow control fractions of 0.0, 2.0, 3.0, 4.0, 4.5 and 5.9%. At 0% flow control, there are several peaks in the standard deviation distribution suggesting that these regions have increased low-frequency unsteadiness. Both the baseline and 2.0% exit flow pattern appear to be predominantly two-dimensional, with some slight endwall deviations being evident.

For increasing flow control, the exit distribution again becomes more three-dimensional, but the region of negligible loss (again, in red) does not extend as far towards the convex surface as either the LSJ-only or short counter-rotating VG configurations. Unlike all three other configurations, the exit distribution maintains a symmetric exit distribution.

At and above 4.0% flow control, there are local pockets of lower total pressure fluid (in green) initially appearing near the convex surface just on either side of the midspan line. These may indicate the location of persisting vortex cores from the tall VGs.

The average velocity field for the 4.0% case was previously documented by DPIV at several spanwise locations and is shown in Figure 9. It is important to point out some differences in the configuration in which the data in this one figure was taken. Though the same Counter-VG-150 upper plate was used, small silicone strips were installed to block about a 3% spanwise portion of the slot area at either end of the slot. In addition, the equivalent throat Mach number was matched at a lower condition, approximately 0.64 instead of 0.7. Despite these differences, interpretation of these three images appear to be consistent with the 4.0% case of Figure 8. At 50% span the flow appears to be attached and well-diffused, while a small region of turbulent flow along the concave surface is suggestive of Görtler vortices (more clear in the unaveraged DPIV images, which are not presented here). At the 75% and 85% span locations there is clear evidence of a three-dimensional endwall separation as the flow abruptly goes from being attached to separated, with streamlines indicative of out-of-plane motion.

A portion of the flow control range between the 4.5% and 5.9% cases was unstable, leading to overall flow unsteadiness, some asymmetry and marginal stability. As the flow control fraction was increased towards 5.9%, however, the bulk flow re-stabilized to a symmetric pattern as shown in Figure 8. This general behavior, as well as the resultant flow pattern, are in contrast to those of the other configurations presently discussed.

The contour plot for this interesting condition is enlarged and rescaled in Figure 10 to provide more detail of the flow pattern. The typically singular low-loss region seems to have split into multiple pockets of relatively high-energy flow, and these are distributed in a symmetric pattern. In addition the pockets of flow with higher loss (i.e. blue) may indicate secondary flows or the locations of persistent vortices from the VGs. Future investigations including stereo DPIV and PSP on the convex surface may be used to elucidate the details of this flowfield.

B. Overall Performance

Attention is now turned to selected metrics of overall performance. Figure 11 provides the area-averaged gage total pressure ratio as defined in Equation (1). At minimum flow control conditions, the CoRot-VG-75 configuration has the lowest total pressure loss (i.e. largest ζ_{Pt}) at 13.5%, followed closely by the Counter-VG-38 version. The Counter-VG-150 configuration shows the greatest loss at 17.7%, which is not surprising in light of the substantial drag producing by the VGs extending above the boundary layer.

From the plot it is also apparent that overall losses increased for all configurations when small nonzero flow control fractions were applied. However, as flow control input was further increased, all configurations demonstrated a net reduction in overall loss. Loss reductions continued to increase to the limit of the tested flow control range.

Similar trends are seen in Figure 12, which shows the static pressure rise coefficient near the end of the diffuser passage. The reader should note, though, that reliability of this calculation is somewhat suspect. It is based on only two static pressure taps (one each per concave and convex sides) which are offset at different spanwise locations. Flow conditions which were especially skewed in their exit profile were omitted from this figure, because they appeared to less accurately quantified by these two pressure taps. Both of these figures suggest that the co-rotating VG configuration was the most promising of those tested until it became unstable and highly skewed.

Global standard deviation of the exit gage total pressure surveys is plotted in Figure 13. This is simply the standard deviation of all normalized exit data points, before any local averaging. It is used here as a

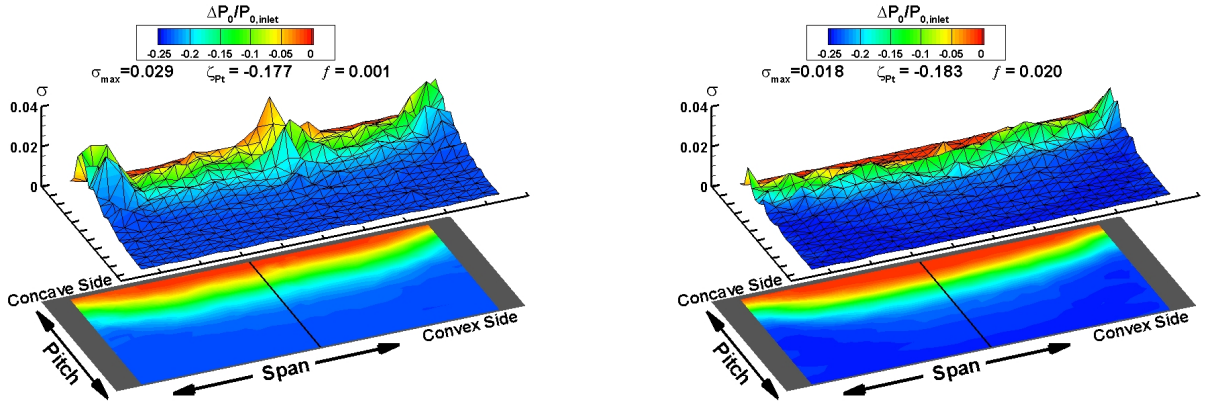

(a) 0.0% (b) 2.0%

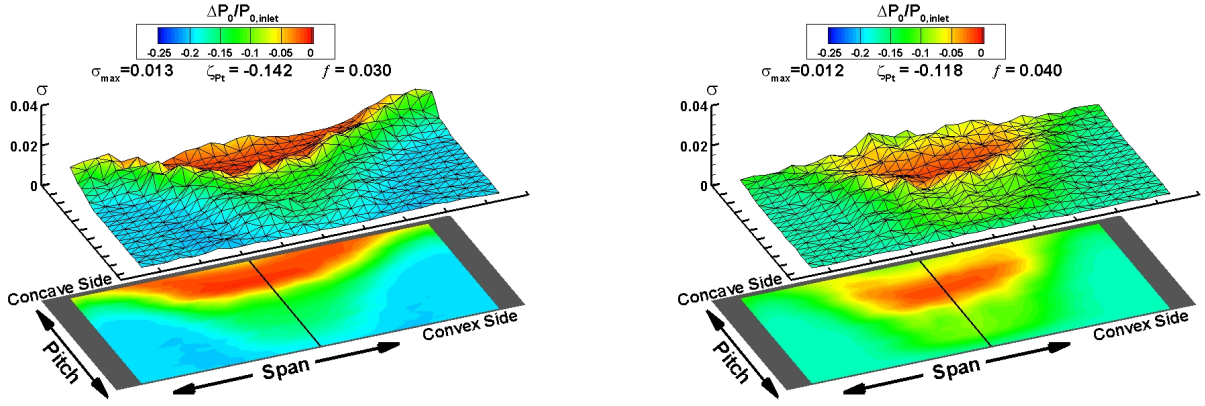

(c) 3.0% (d) 4.0%

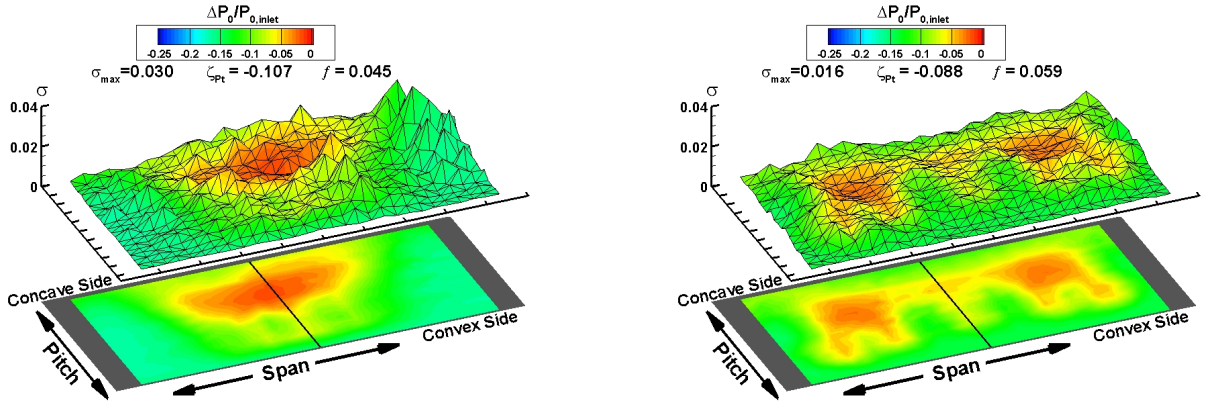

(e) 4.5% (f) 5.9%

Figure 8. Contours of Exit Gage Total Pressure Ratio for varying Flow Control with Counter-Rotating VGs (150% BL height).

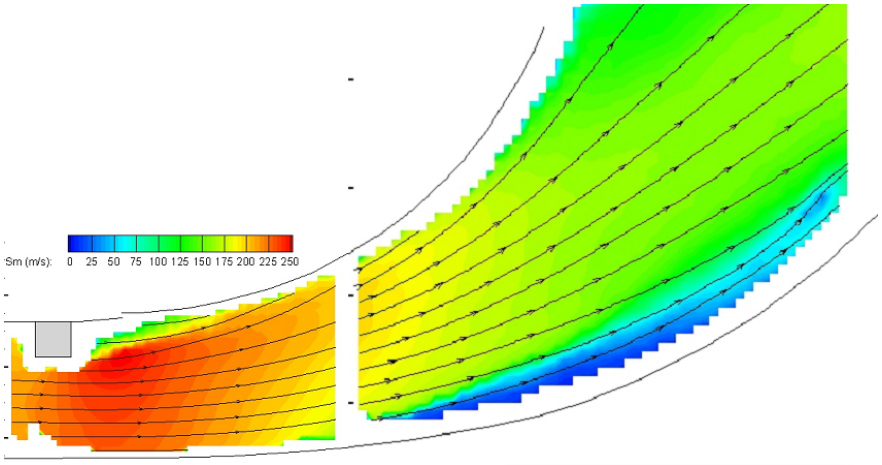

(a) 50% Span

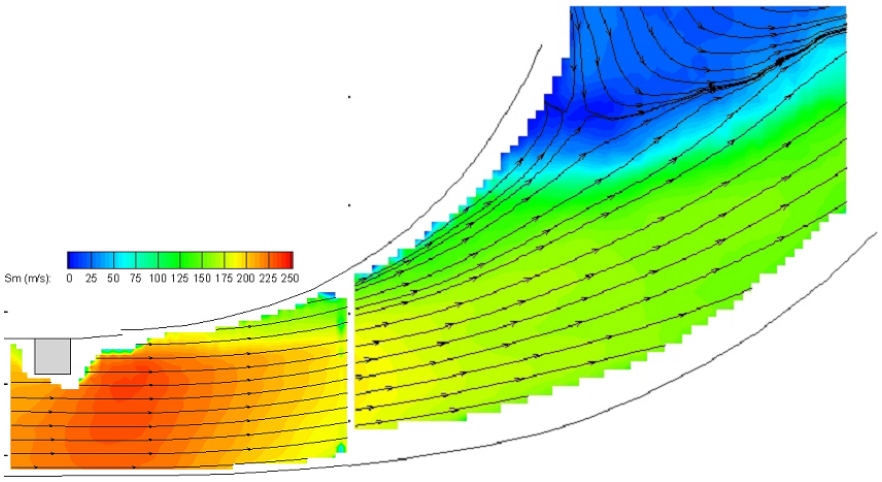

(b) 75% Span

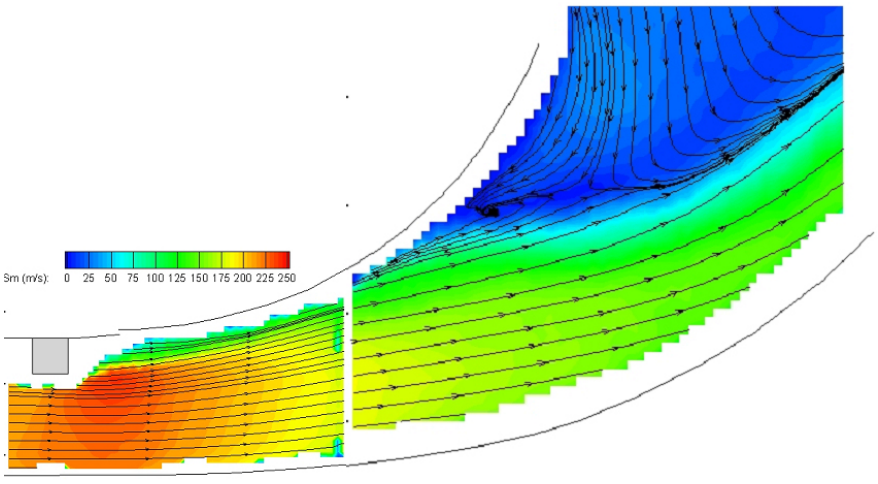

(c) 85% Span

Figure 9. Averaged DPIV velocity field at varying span for Counter-Rotating VGs (150%) and 4% flow control (see related discussion for important notes on this data).

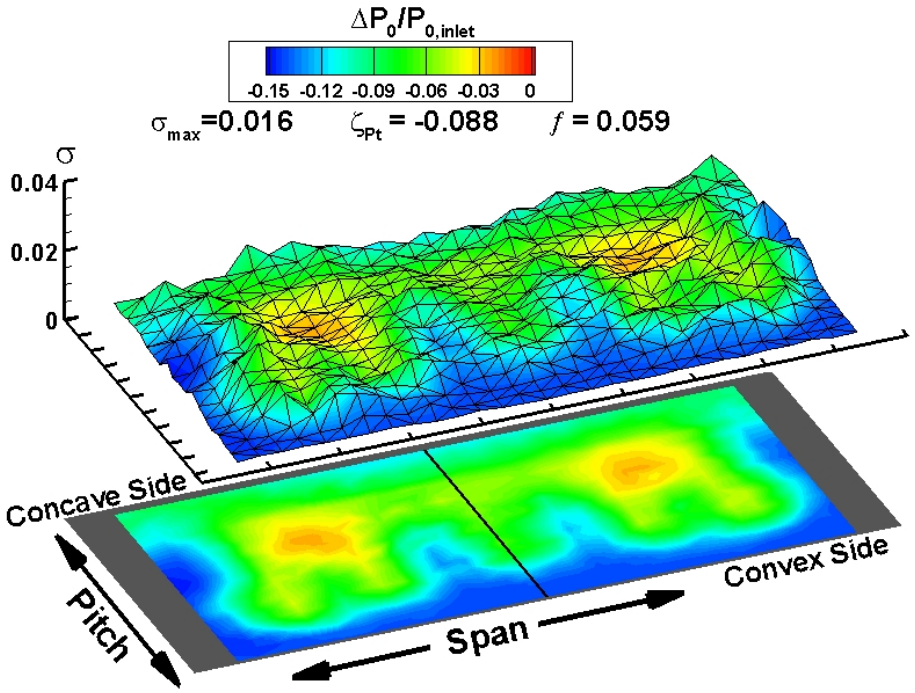

Figure 10. Contours of Exit Gage Total Pressure Ratio for 5.9% Flow Control with Counter-Rotating VGs (150% BL height).

crude collective indicator of the flowfield spatial uniformity and temporal steadiness. In most cases, temporal unsteadiness was low, so this figure can be generally interpreted as an inverse measure of the exit spatial uniformity.

All of the configurations show an eventual improvement in the uniformity for increasing flow control. However, global standard deviation of the first three characteristics trends upward at the highest flow fractions, coincident with their respective shifts toward highly skewed profiles. Only the Counter-VG-150 configuration continues to improve in flowfield uniformity, with the interesting pattern at 5.9% having substantially lower standard deviation (3.5%) than that of the lowest of the other configurations (5.4%).

VI. Conclusions

The effectiveness of linear slot jet flow control for diffusion enhancement in a curved passage was experimentally evaluated with and without the presence of vortex generators (VGs). Several VG configurations were tested, including two designs producing pairs of counter-rotating vortices, and one version producing arrays of co-rotating vortices.

At baseline conditions (minimum slot jet flow), the shorter VG designs were found to provide some diffusion enhancement and loss reduction compared to the non-VG configuration, whereas the tall counter-rotating VGs exhibit an increase in loss. With the addition of slot jet flow, all configurations showed an initial decline followed by a net increase in performance of similar magnitude, with choked slot jet flows tending to lead to flow instabilities.

Upon further increases in slot jet flow, all configurations eventually achieved a stable flow pattern, though three configurations produced highly asymmetric exit flow distributions. The co-rotating VG design showed favorable performance with and without slot flow, but reached stability limits before other configurations. Only the tall counter-rotating VG configuration produced a symmetric exit flow at high flow control inputs. A noteworthy change in the flow pattern, with substantially improved uniformity, is documented near 6% flow control input and will be the subject of more detailed investigation.

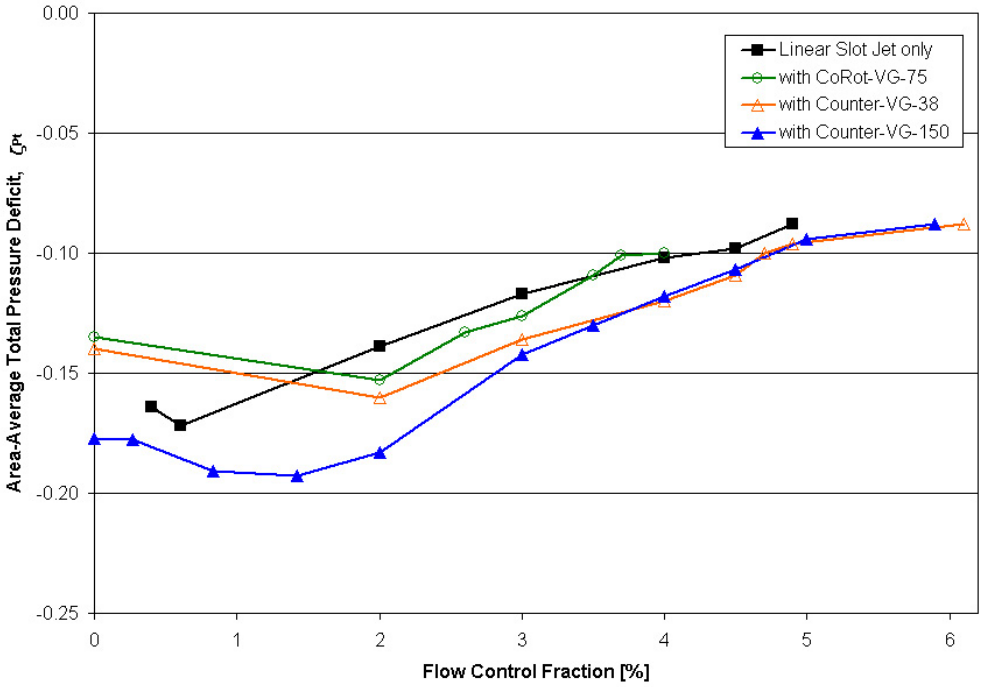

Figure 11. Effect of flow control on total pressure losses.

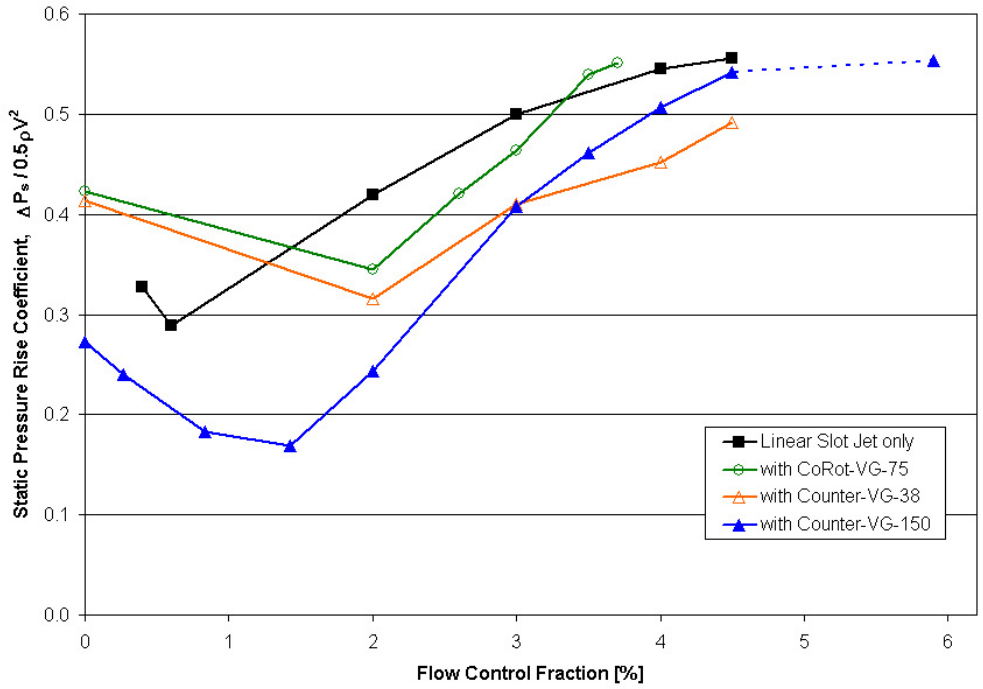

Figure 12. Effect of flow control on static pressure rise coefficient.

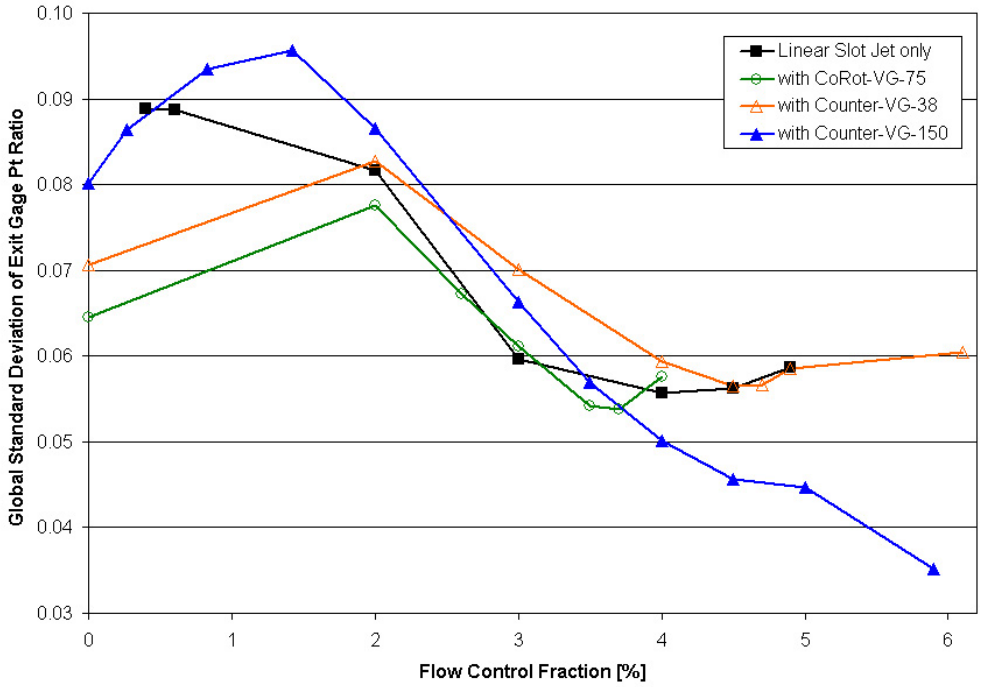

Figure 13. Effect of flow control on global standard deviation of exit total pressure ratio.

VII. Acknowlegements

The authors would like to thank the Air Force Office of Scientific Research (AFOSR) for funding these investigations.

References

[1]Schuler, B. J., Kerrebrock, J. L., and Merchant, A., "Experimental Investigation of a Transonic Aspirated Compressor," *ASME Journal of Turbomachinery*, Vol. 127, April 2005, pp. 340–348.

[2]Merchant, A., Kerrebrock, J. L., Adamczyk, J. J., and Braunscheidel, E., "Experimental Investigation of a High Pressure Ratio Aspirated Fan stage," *ASME Journal of Turbomachinery*, Vol. 127, January 2005, pp. 43–51.

[3]Luedke, J., Graziosi, P., Kirtley, K., and Cerretelli, C., "Characterization of Steady Blowing for Flow Control in a Hump Diffuser," *22nd Applied Aerodynamics Conference and Exhibit*, Providence, RI, 2004, AIAA Paper no. 2004-4963.

[4]Kirtley, K. R., Graziosi, P., Wood, P., Beacher, B., and Shin, H. W., "Design and Test of an Ultra-Low Solidity Flow-Controlled Stator," *ASME Turbo Expo 2004*, Vienna, AU, 2004, ASME Paper no. GT2004-53012.

[5]Harff, M. R., Wolff, J. M., Copenhaver, W. W., Car, D., and Estevadeordal, J., "Stator Cascade Flow through Counter-flow Blowing," *21st Applied Aerodynamics Conference*, Orlando, FL, 2003, AIAA Paper no. 2003-3408.

[6]Carter, C. J., Guillot, S. A., Ng, W. F., and Copenhaver, W. W., "Aerodynamic Performance of a High-Turning Compressor Stator with Flow Control," *37th AIAA/ASME/SAE/ASEE Joint Propulsion Conference & Exhibit*, Salt Lake City, UT, 2001, AIAA Paper no. 2001-3973.

[7]Lord, W., MacMartin, D. G., and Tillman, T. G., "Flow Control Opportunities in Gas Turbine Engines," *Fluids 2000*, Denver, CO, 2000, AIAA Paper no. 2000-2234.

[8]Car, D., Bailie, S. T., Baudendistel, C. M., Gebbie, D., and Estevadeordal, J., "Fluidic Control Studies for Diffusion Enhancement in Axial Compression Systems," *44th Aerospace Sciences Meeting and Exhibit*, Reno, NV, 2006, AIAA Paper no. 2006-0417.

[9]Pearcey, H. H., "Shock Induced Separation and Its Prevention by Design and Boundary Layer Control," *Boundary Layer and Flow Control*, edited by G. V. Lachmann, Vol. 2, Pergamon Press Inc., New York, 1961, pp. 1170–1349.

[10]McLachlan, B. G., "Study of a Circulation Control Airfoil with Leading/Trailing-Edge Blowing," *Journal of Aircraft*, Vol. 26, September 1989, pp. 817–821.

[11]Fiedler, R. A. and Gessner, F. B., "Influence of Tangential Fluid Injection on the Perfomance of Two-Dimensional Diffusers," *ASME Journal of Basic Engineering*, September 1972, pp. 666–674.

[12]Ball, W. H., "Experimental Investigation of the Effects of Wall Suction and Blowing on the Performance of Highly Offset Diffusers," *19th AIAA/SAE/ASME Joint Propulsion Conference*, Seattle, WA, 1983, AIAA Paper no. 83-1169.

[13]Kwong, A. H. M. and Dowling, A. P., "Active Boundary–Layer Control in Diffusers," *AIAA Journal*, Vol. 32, No. 12, 1994, pp. 2409–2414.

[14]Lin, J. C., Selby, G. V., and Howard, F. G., "Exploratory Study of Vortex-Generating Devices for Turbulent Flow Separation Control," *29th Aerospace Sciences Meeting*, Reno, NV, 1991, AIAA Paper no. 91-0042.

[15]Schoppa, W., Hussain, F., and Metcalfe, R. W., "A New Mechanism of Small-scale Transition in a Plane Mixing Layer: Core Dynamics of Spanwise Vortices," *Journal of Fluid Mechanics*, Vol. 298, 1995, pp. 23–80.

[16]Amitay, M. and Cohen, J., "Instability of a Two-dimensional Plane Wall Jet Subjected to Blowing or Suction," *Journal of Fluid Mechanics*, Vol. 344, 1997, pp. 67–94.

[17]Khan, Z. U. and Johnston, J. P., "On Vortex Generating Jets," *International Journal of Heat and Fluid Flow*, Vol. 21, 2000, pp. 506–511.

[18]Vukasinovic, B., Lucas, D. G., and Glezer, A., "Direct Manipulation of Small-Scale Motions in a Plane Shear Layer," *2nd AIAA Flow Control Conference*, Portland, OR, 2004, AIAA Paper no. 2004-2617.

[19]Schubauer, G. B. and Spangenberg, W. G., "Forced Mixing in Boundary Layers," *Journal of Fluid Mechanics*, Vol. 8, 1960, pp. 10–32.

[20]Kuethe, A. M. and Chow, C.-Y., *Foundations of Aerodynamics: Bases of Aerodynamic Design*, John Wiley & Sons, 4th ed., 1986.